ORIGINAL ARTICLE

On the fatigue notch sensitivity of Ti6Al4V specimens with $\alpha + \beta$ microstructure produced by laser powder bed fusion

Antonio Cutolo[1-2] | Chola Elangeswaran[1-2] | Gokula Krishna Muralidharan[3] | Brecht Van Hooreweder[1]

[1]KU Leuven Department of Mechanical Engineering, Celestijnenlaan 300, 3001 Leuven (Heverlee), Belgium

[2]SIM M3 Program, Technologiepark 48, 9052 Zwijnaarde, Belgium

[3]3D Systems Leuven, Grauwmeer 14, 3001, Leuven, Belgium

Correspondence
Brecht Van Hooreweder, KU Leuven Department of Mechanical Engineering, Celestijnenlaan 300, 3001 Leuven (Heverlee), Belgium
Email: brecht.vanhooreweder@kuleuven.be

Funding information
SIM (Strategic Initiative Materials in Flanders) VLAIO (Flemish government agency, Flanders Innovation & Entrepreneurship), M3-FATAM project (HBC.2016.0446), part of the MacroModelMat (M3) research program, coordinated by Siemens (Siemens Digital Industries Software, Belgium

Laser powder bed fusion (L-PBF) is an additive manufacturing (AM) process which offers several advantages over conventional manufacturing techniques, including material savings and design possibilities. For these reasons several industrial sectors such as biomedical, aerospace and automotive, are considering L-PBF for customized parts production. Among the processable material palette, Ti6Al4V gained increasing interest due to the high specific strength, and stiffness, and excellent bio-compatibility, and corrosion resistance. However, to include L-PBF Ti6Al4V parts in load bearing applications it is important to properly understand the mechanical properties of AM'ed materials with a specific focus on fatigue behaviour. In this study the fatigue notch sensitivity of Ti6Al4V L-PBF manufactured specimens is investigated in depth. Samples with different notches were subjected to stress relieving heat treatment to generate a fine $\alpha + \beta$ microstructure. The results were used to define a relation between the perturbed stress field generated by the geometrical discontinuity, the microstructure size and the notch sensitivity. Moreover, the critical distance has been calculated using the theory of critical distance formulated with the line method (LM). The estimated value were adopted to predict fatigue properties of notched components with different notch radii.

KEYWORDS
laser powder bed fusion - Ti6Al4V - fatigue properties - notch sensitivity - critical distance

List of symbols and abbreviations

ρ	notch radius
σ_1	maximum principal stress
σ_a	stress amplitude for plain specimens
σ_{a-n}	stress amplitude for plain specimens
σ_f	fatigue strength
σ_{eff}	effective stress calculated using the theory of critical distance
k_f	fatigue notch factor
k_t	stress concentration factor
k_{th}	threshold stress intensity factor
l_0	critical distance
N_f	number of cycles to failure
$N_{5\%}$	number of grains within 5% of the maximum stress
N_{fE}	experimental number of cycles to failure
N_{fp}	predicted number of cycles to failure
q	notch sensitivity factor
R	stress ratio
r	distance from the notch root
S_a	stress reduction across one grain
AM	additive manufacturing
TCD	theory of critical distance
L-PBF	laser powder bed fusion
LM	line method

1 | INTRODUCTION

Additive manufacturing (AM) techniques are becoming more and more popular and, in some cases, replacing conventional manufacturing processes for end-use parts. This is typically the case when high design freedom is required and when complex geometries need to be fabricated. Due to this ability to fabricate customized components with limited geometrical constraints, AM techniques are increasingly being used in several industrial sectors such as aerospace, biomedical and automotive. Among these processes, laser powder bed fusion (L-PBF) allows manufacturing of the workpiece in a layer-by-layer fashion, melting successive powder layers using a high-power laser [1].

One of the major drawbacks of powder bed AM processes is the poor surface quality of the as-produced parts. For demanding applications, typically, post-machining operations are still needed to meet specific tolerances and to

improve mechanical performance. In fact, in order to include AM components in load bearing applications, the fatigue properties of the parent material need to be carefully evaluated.

Although the last decade has seen an increasing interest on the correlation between fatigue behaviour and process parameters, defects, microstructure ([2, 3, 4, 5, 6]) the state of the art is lacking of correlation between fatigue data of test coupons and fatigue performances of final parts with complex geometry. A first attempt has been proposed by Molaei et al. [7] in which the authors related fatigue performances of Ti6Al4V specimens with the ones of an aircraft link component. The component studied consists of a relative simple geometry in which no severe geometrical discontinuities were present. Therefore Molaei et al. suggested that any stress gradient effect was negligible hence there was no need to include the influence of the stress gradient on the component fatigue performances.

However, geometrical discontinuities will be present in most AM design. This is usually the case of components design resulting from topology optimization process after which the resulting geometry may consists of complex shapes and features. In those cases, the geometrical discontinuities can be responsible for stress concentrations which can lead to premature failure. Therefore an increasing interest in fatigue behaviour of notched AM components has been reported during the last years.

One of the first works related to AM Ti6Al4V notch-sensitivity was performed by Kahlin et al. [8] who studied notched specimens in both as-produced and machined surface condition produced by electron beam melting (E-PBM) and L-PBF techniques. Kahlin et al. reported that L-PBF and E-PBM produced material showed similar fatigue behaviour for specimens with geometrical notches with a stress concentration factor $k_t = 2.5$ with machined surface and stress relieved volume post-treatment. This behaviour is most likely due to a volume effect in which the crack initiation site is guided by internal pores and lack of fusion defects. Therefore Kahlin et al. suggested to perform hot isostatic pressing (HIP) so to reduce or eliminate internal defects. By performing HIP to E-PBF Ti6Al4V specimens, the authors reported a fatigue notch sensitivity similar to wrought Ti6Al4V bar even though a significant difference in material microstrucure is to be expected.

Razavi et al. [9] performed a study on L-PBF Ti6Al4V notch sensitivity on specimens with as-produced surface condition and reported a low notch sensitivity. This result is attributed to the fact that the high surface roughness overshadowed the effect of the geometrical discontinuity. In a more recent study, Razavi and Berto [10] compared fatigue performances of Ti6Al4V with a fine Widmanstätten $\alpha+\beta$ microstructure obtained via direct energy deposition (DED-LENS) AM technique with wrought coarse equiaxed α grains for both plain and notched specimens. Due to the poor surface quality of the as-produced LENS parts, Razavi and Berto investigated specimens in machined surface condition. Both in the case of plain and notched specimens, the AM specimens showed superior fatigue performances if compared to conventionally manufactured parts. In case of LENS specimens the fatigue failure always initiated at the surface with no influence of internal defects on to dynamic properties. Therefore Razavi and Berto were able to relate the critical distance to microstructural features. The enhanced fatigue performances were attributed to the different microstructure morphology with the finer $\alpha + \beta$ Ti6Al4V microstructure generated by LENS outperforming

the coarse equiaxed Ti6Al4V α grains. A similar conclusion was also reported by Cutolo et al. [11] for plain Ti6Al4V L-PBF specimens that underwent different heat treatments. The authors reported superior fatigue performances for Ti6Al4V specimens with a fine $\alpha + \beta$ microstructure.

Benedetti et al. [12] investigated the notch sensitivity of L-PBF Ti6Al4V with a fine $\alpha + \beta$ microstructure. In their study Benedetti et al. tried to combine the notch sensitivity with the defect sensitivity as the specimens produced presented large pores and lack of fusion defects. Although the predictions based on the critical distance were promising it wasn't possible to separate the defect sensitivity from the notch sensitivity. Similar conclusions on the combination of notch and defect sensitivities were reported in a recent study by Molaei et al. [13] in which the AM Ti6Al4V notch sensitivity under axial and multi-axial loading conditions was investigated.

As AM machine builders are improving the machine quality and the process stability [14], resulting parts are more and more defect free, making it also important to evaluate material fatigue properties in function of the peculiar microstructures generated by the different AM processes.

In the present study the fatigue properties of Ti6Al4V specimens produced by L-PBF in presence of geometrical discontinuities are investigated. Before testing, all the samples underwent a stress relieving heat-treatment followed by surface machining. Three different notch geometries were investigated and their fatigue performances were compared to one plain geometry. Given to the high quality of the coupons, the dynamic performances were not affected by internal defects so to directly relate the notch sensitivity to the material microstructure through two empirical relations between grain size, stress field and fatigue strength. Moreover, material critical distance has been evaluated via different theories of critical distance (TCD). Results show a good agreement between the investigated methodologies. The calculated values are in line with the critical distances evaluated via threshold stress intensity factor measurements reported in literature [12]. Besides, the critical distance has been used to predict the fatigue properties of notched components with different notch radius. The results obtained showed the importance of accounting for notch size effect in predicting fatigue performances.

2 | MATERIALS AND METHODS

The test coupons used in this investigation were produced via L-PBF ProX320 system (3D Systems) equipped with a $500W$ fiber-laser and a vacuum chamber to reduce the oxygen levels during production. Hexagonal bars and quasi-static test coupons were produced using LaserForm Ti Gr23 powder (3D Systems) for Ti6Al4V specimens. The powder chemical composition is presented in Table 1. A layer thickness of $60\mu m$ and optimized production parameters were used for the manufacturing [14].

The bars and the quasi-static test specimens were produced with the axis oriented in the building direction. Special attention was given to avoid any oxygen pickup during manufacturing of the titanium samples by flushing the build chamber with argon and by keeping oxygen levels in the build chamber below $50ppm$.

TABLE 1 LaserForm Ti Gr23 powder (3D Systems) chemical composition [15]

Element	Ti	Al	V	Fe	O	C	H	N	Y
Weigth [%]	Bal.	5.5 – 6.5	3.5 – 4.5	< 0.25	< 0.13	< 0.08	< 0.012	< 0.03	< 0.005

After the production, a stress relieving operation consisting of heating the coupons to a temperature of 850°C for $2h$ and followed by air cooling was performed. This process was intended to relieve any type of residual stress developed during the manufacturing process. The hexagonal bars then were subjected to machining operation to generate the 4 different specimen geometries of Figure 1, i.e. one plain and three notched geometries. For the plain specimens a miniaturised coupon geometry (Figure 1a) specifically designed to assess the fatigue properties of additively manufactured metals was selected [11, 16, 5]. According to the specimen geometry the samples were divided in 4 batches, i.e. plain, $k_t = 1.58$, $k_t = 2.19$ and $k_t = 3.09$. The machining process aimed to a fine surface finish with an average value of the surface roughness, i.e. R_a, lower than $0.2\mu m$.

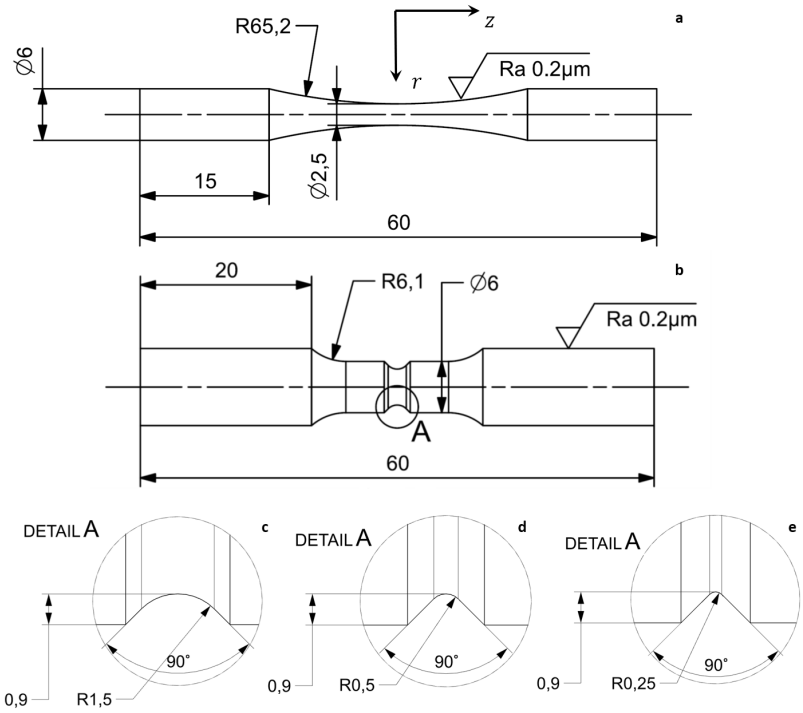

FIGURE 1 Test specimen geometries: a) plain coupons; b) notched coupons; Geometries for notch factor c) $k_t = 1.58$; d) $k_t = 2.19$; e) $k_t = 3.09$; all dimensions are in mm

The three values of the stress concentration factors of the three different notched geometries were calculated using finite element (FE) linear elastic analysis. The models were meshed with quadratic tetrahedral elements. A mesh

convergence analysis was performed on the model with $\rho = 0.25mm$ to ensure that a proper element size was used for the FE simulations. The maximum principal stress has been considered as the key parameter for the convergence study. A minimum element size of $2.5\mu m$ was used to discretize the notched region. Young's modulus and Poisson's ratio were set equal to $132GPa$ and 0.34 respectively. The models were simulated under a tensile load condition that generates a nominal stress of $1MPa$ across the smallest cross section. The radial stress distribution along the smaller cross section was used to calculate the critical length according to the theory of critical distance (TCD) expressed, for the line method (LM), by following equation:

$$\sigma_{eff} = \frac{1}{2l_0} \int_0^{2l_0} \sigma_1(r)\, dr \tag{1}$$

where σ_{eff} is the effective stress, l_0 is the critical distance, σ_1 is the principal stress, r represents the distance from the notch root. In the LM the stress is determined by averaging along a line L starting at the notch-root. The length of this line is related to the critical distance by the relation: $L = 2l_0$ [17].

The samples were sectioned along a plane perpendicular to the building direction to observe the microstructure. Optical microscopy was performed with Keyence VHX-6000 on ground, polished and etched samples. Modified Keller's reagent ($95mL\ H_20$, $2.5mL\ HNO_3$, $1mL\ HCI$, $1.5mL\ HF$) was used to etch the samples. The optical microscopy images were analysed via ImageJ software to measure the α width.

Quasi-static tensile tests were performed on an INSTRON 3360 machine equipped with a $30kN$ load cell according to ASTM E8M standard for evaluating static properties of the L-PBF Ti6Al4V.

Fatigue tests were performed according to the ASTM E466. The tests were force-controlled and conducted with a constant amplitude fully reversed sinusoidal load (stress ratio $R = -1$) with a frequency of $60Hz$.

For each batch, at least 4 different stress levels were investigated and, for each stress level, at least three samples were tested. Fatigue tests were performed on the 4 different batches until failure of the sample or stopped if no failure occurred after 10^7 cycles. The samples that survived 10^7 cycles were tested a second time with a higher value of the stress amplitude to determine the material fatigue strength at 10^7 cycles according to the step procedure described by Nicholas et.al. [18] and validated by Bellows et. al. [19] for conventionally manufactured Ti6Al4V.

A Philips XL 30 FEG scanning electron microscope (SEM) was used for crack initiation points identification on fractured samples.

TABLE 2 L-PBF Ti6Al4V properties

Young's modulus	Strain at Yield	Yield stress	Strain at maximum stress	Maximum stress	Maximum strain	α width
(GPa)	(%)	(MPa)	(%)	(MPa)	(%)	(μm)
132.40 ± 9.10	0.92 ± 0.05	914.27 ± 7.65	10.15 ± 0.27	999.32 ± 4.72	17.08 ± 1.01	1.19 ± 0.21

3 | RESULTS AND DISCUSSION

| Microstructure and quasi-static properties

The results of the optical microscopy, shown in Figure 2, highlight that a fine $\alpha + \beta$ Widmanstätten microstructure is obtained after the stress relieving operation. This microstructure results from the decomposition of the typical L-PBF process-induced α' acicular martensitic microstructure to $\alpha + \beta$ [20, 21]. In a Widmanstätten/basketweave microstructure, the lamellar width is considered as the effective grain size. The average values of the grain size are reported in Table 2. The measured values are in line with the measurements performed by Vrancken et.al. [21] on L-PBF Ti6Al4V subjected to the same heat treatment cycle (i.e. 850°C for two hours followed by air cooling).

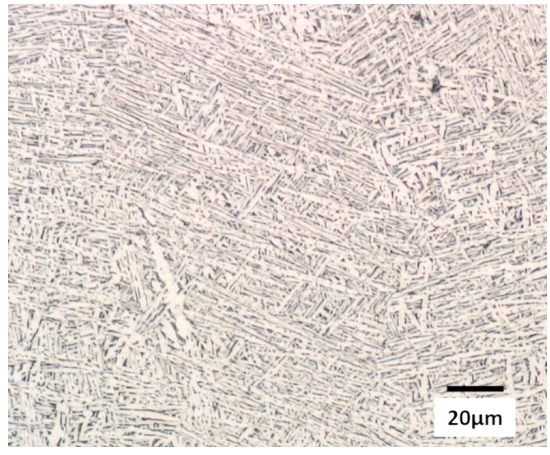

FIGURE 2 L-PBF Ti6Al4V $\alpha + \beta$ microstructure obtained after stress-relief heat treatment

The quasi-static tensile test results are presented in Table 2. The transformation of the α' to a fine dual phase $\alpha+\beta$ microstructure generated during the heat treatment guarantees a good compromise between strength and ductility.

Numerical simulations

In order to understand the fatigue behaviour of notched components with respect to the plain coupons it is important to evaluate the local stress distribution in the proximity of the notch root. In this regard, linear elastic FE analysis was performed under axial loading condition. Due to the double symmetry, the numerical models consist of one fourth of the geometry presented in Figure 1b. The numerical simulations results of the three different notch geometries indicate that the three discontinuities generate a stress re-distribution across the smallest cross section with a stress concentration at the notch root. An example of the FE numerical simulation results is presented in Figure 3a, in which the geometry with the smallest radius, i.e. $\rho = 0.25mm$, was analysed. Figure 3a shows the principal stress distribution calculated for an applied load that generate a nominal stress of $1MPa$ across the smallest cross section. The graphs in Figure 3b show the maximum principal stresses in function of the distance from the notch root towards to the centre of the model along the radial direction for the three notch geometry (direction r indicated in Figure 3a). By dividing the maximum value of the maximum principal stress by the nominal stress across the smallest section it was possible to estimate the stress concentration factor k_t for the three notch geometries, i.e. $k_t = 1.58, k_t = 2.19, k_t = 3.09$, corresponding to the notch radii of $1.50mm, 0.50mm, 0.25mm$, respectively.

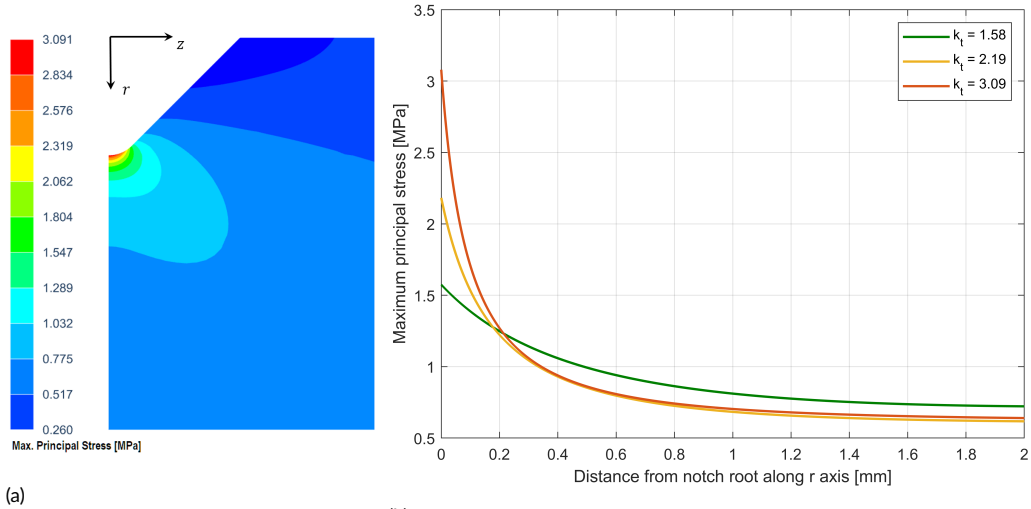

FIGURE 3 a) normalized principal stress distribution for $k_t = 3.09$; b) normalized principal stress in function of the distance from the notch root for the three notched geometries

As presented in Figure 3b, the three notch radii generate different stress distributions with $\rho = 1.50mm$ generating a smoother transition from the peak stress to the stress plateau if compared to $\rho = 0.50mm$ and $\rho = 0.25mm$. On the contrary the latter two geometries induce similar stress distributions with a steeper transition from the peak stress to the stress plateau. The curves presented in Figure 3b have been fitted with 2^{nd} degree polynomial rational functions

TABLE 3 Eq.3 fitting coefficients for of the un-notched and notched specimens

k_t	a	b	c	R^2
Plain	494.3	4156	0.3004	0.75
1.58	378.2	$2.44E+4$	0.4503	0.83
2.19	319.7	$3.18E+4$	0.5905	0.91
3.09	272.6	$1.84E+4$	0.5637	0.96

of the type presented by eq. 2 using non-linear least square fitting in which the variable r represents the distance from the notch root along the axis r of Figure 3a.

$$\sigma_1(r) = \frac{p_1 r^2 + p_2 r + p_3}{r^2 + q_1 r + q_2} \tag{2}$$

Substituting this function in eq. 1 for the smaller notch radius ($\rho = 0.25mm, kt = 3.09$) the critical distance can be calculated with the line method. The formulation expressed by eq. 2 has been used for the stress-gradient calculation at the notch root for the three notch radii.

| Fatigue test results

Experimental fatigue tests results are presented in Figure 4. The data are fitted using the following equation:

$$\sigma_a(N_f) = a + \frac{b}{N_f^c} \tag{3}$$

in which σ_a is the stress amplitude, N_f indicates the number of cycles to failure and a, b and c are three fitting coefficients determined by non-linear least square fitting of the experimental data. The details of the fitting parameters are presented in Table 3. The goodness of the fit is indicated by the R^2 column.

For the plain specimens a fatigue strength of $495MPa$ at 10^7 cycles was calculated using the step procedure [18]. As expected, the fatigue life in low and high cycles regime was reduced in presence of notches with $k_t = 3.09$ batch showing the lowest fatigue behaviour. Fatigue strength at 10^7 cycles of 379, 321 and $273MPa$ were obtained, respectively, for $k_t = 1.58$, $k_t = 2.19$ and $k_t = 3.09$.

By using the SN curves of Figure 4 obtained via eq. 3, the fatigue notch factor k_f in function of the number of cycles to failure has been calculated with the following equation:

$$k_f(N_f) = \frac{\sigma_a(N_f)}{\sigma_{a-n}(N_f)} \tag{4}$$

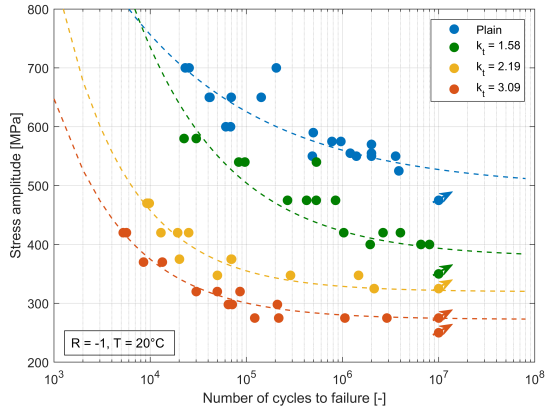

FIGURE 4 Fatigue test results for plain and notched L-PBF Ti6Al4V specimens.

Applying this equation to the fitted SN curves of Figure 4 yields the graph presented in Figure 5.

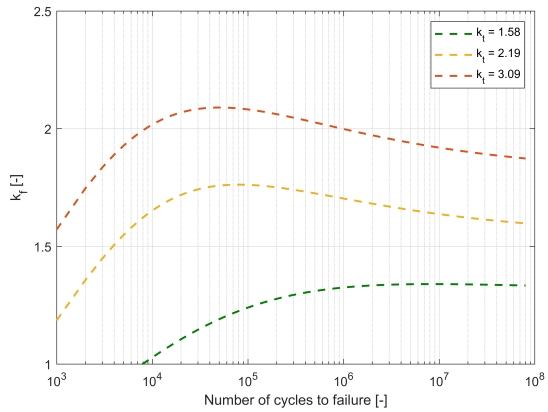

FIGURE 5 Fatigue notch factors in function of the number of cycles to failure

Figure 5 shows that the fatigue notch factor increases with the stress concentration factor in the entire fatigue life range. However two different behaviours can be noticed. For high values of the k_t the fatigue notch factor has a maximum value in the range $[10^4–10^5]$ cycles and then decreases with the increase of the number of cycles to failure. On the other hand, for low k_t values the maximum k_f is reached at very high cycle fatigue.

| Fractured surface analysis

SEM pictures of fractured surfaces of notched specimens are presented in the Figure 6. From the fractographic analysis it is noted that for the three notch geometries analysed in this work, fatigue cracks initiate at the specimen

surface and more specifically at the root of the notch. This confirms indeed the high sample quality and the fact that failure of the test coupons was not initiated by internal pores or lack of fusion defects.

For $k_t = 1.58$, fatigue initiation occurred at a single point on the external surface (Figure 6a and 6b) and propagated to the opposite side covering almost the entire cross section until the final rupture (Figure 6a). Similar behaviour is observed also for $k_t = 2.09$ (see Figure 6c and 6d). The final fractured surfaces were found to be inclined at 45° with respect to the load direction.

For $k_t = 3.09$ fatigue cracks initiated at multiple points along the external surface. The final fracture appeared in between the multiple propagation areas and it was found to be inclined at 45° with respect to the load direction. In Figure 6e and 6f representative SEM pictures of this behaviour are presented with Figure 6e showing three different initiation sites.

| Critical distance

The critical distance has been evaluated using the TCD formulated with the line method (i.e. eq. 1) in the entire fatigue life range as proposed by Susmel and Taylor [22]. The authors re-formulate the TCD so as to predict notch components' fatigue life in the low, medium and high cycle regime. According to this procedure it is possible to define the critical distance in function of the number of cycles to failure. To achieve this, two calibration SN curves are needed: one generated for plain, non-notched samples and one obtained by testing notched specimens. For the present study the SN curves of plain and kt = 3.09 specimens were considered as calibration curves. Since the SN curves have been expressed using eq. 3, in the present study the relation between critical distance and the number of cycles to failure has been expressed as an equation with a similar fashion:

$$l_0(N_f) = A + \frac{B}{N_f^C} \tag{5}$$

The results are presented in Figure 7 in which an asymptotic tendency of l_0 can be observed with the increase of N_f. Another attempt to evaluate the critical distance has been performed using the methodology recently proposed by Santus et al. [23]. Santus et al. proposed a strategy for the evaluation of the material critical distance using notched components without fracture mechanics tests aimed at measuring the threshold stress intensity factor range. As alternative, Santus et al. considered a dedicated analytical formulation to calculate the critical distances using both the line and point method. Applying Santus et al.'s methodology yields to the results presented in Figure 7.

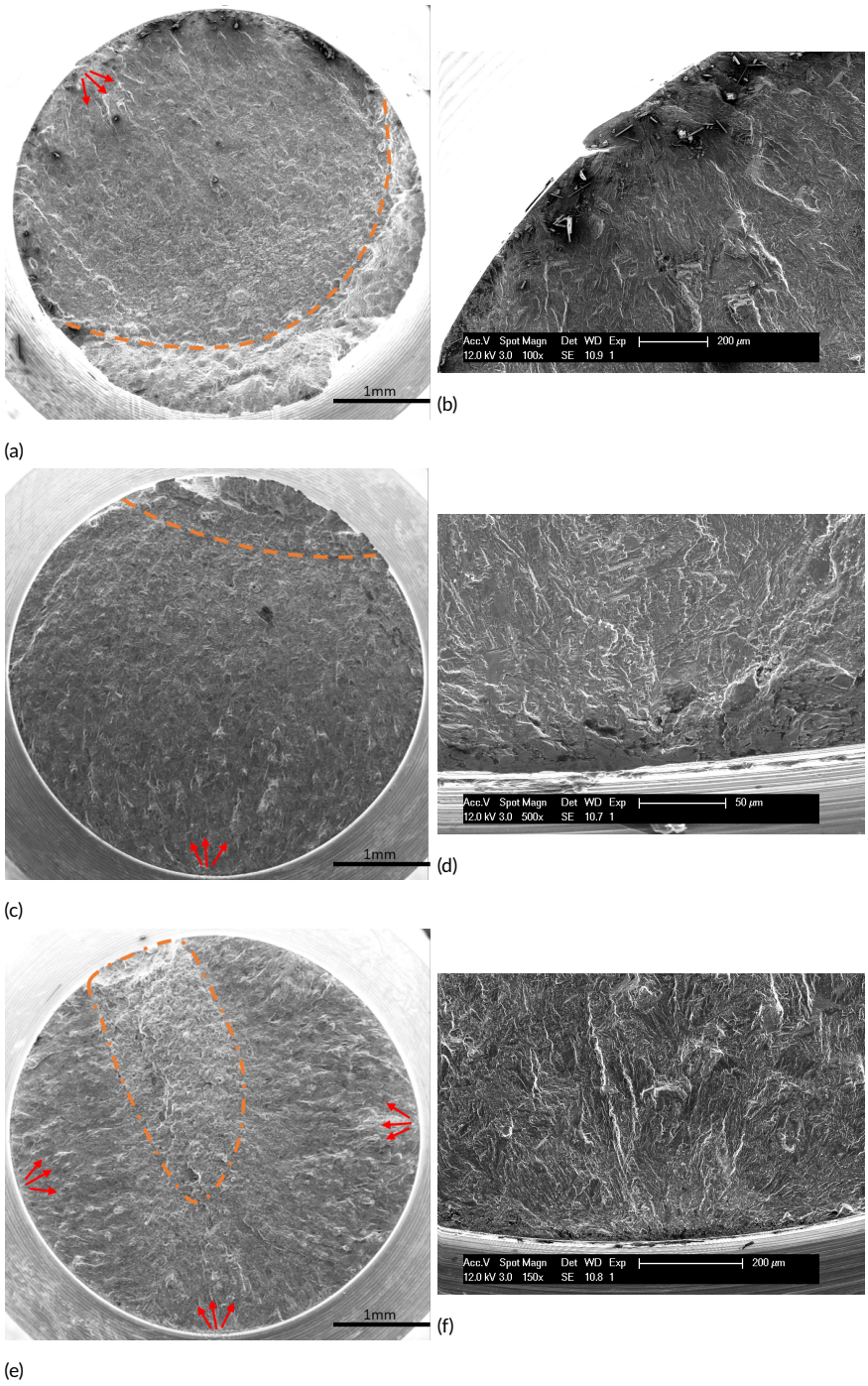

FIGURE 6 Representative fractured surfaces SEM images the three different notched specimens: $k_t = 1.58$ a) and b); $k_t = 2.19$ c) and d); $k_t = 3.09$ e) and f)

A good agreement between the two methodologies used for the critical distance evaluation can be noticed especially in the high cycle fatigue range.

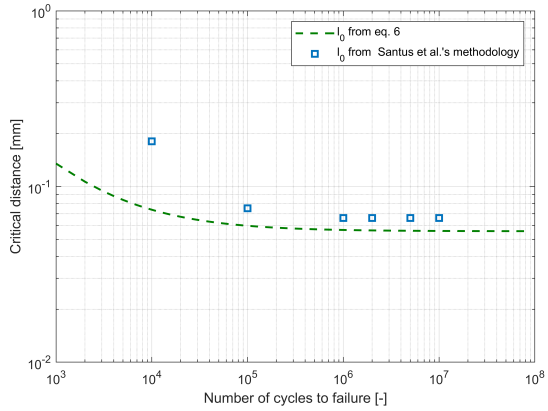

FIGURE 7 Critical distance in function of the number of cycles to failure calculated according to eq. 5 and to [23]

Although Santus et al.'s procedure was found to be very accurate for conventional manufactured components [24], it was not possible to obtain the same results for additively manufactured metals. In fact, Benedetti et al. [12] used Santus et al.'s methodology for critical distance evaluation of L-PBF Ti6Al4V and the calculated values were far off from the ones evaluated using conventional threshold stress intensity factor. Benedetti et al. attributed this deviation to the presence of defects, generated during the manufacturing process, that perturb the stress field at the notch root overshadowing the notch sensitivity. The critical distance values reported by Benedetti et al. were calculated under the assumption of a homogeneous continuum material which generates the mentioned error. The presence of large defects resulted in longer critical distance and a lower notch factor and sensitivity factor q.

In Table 4 the values of the critical distances for $N_f = 10^7$ cycles calculated in this study are compared with the ones of Benedetti et al. obtained using Santus et al.'s methodology and the stress intensity factor measurements. This comparison can be made because the AM process, material, and microstructure presented here is similar to the one reported by Benedetti et al. [12]. Due to the fact that no defects were found to be responsible for the crack initiation of the notched components, it was possible to obtain a good agreement between the calculated critical distances and the one obtained by Benedetti et al. [12] via threshold stress intensity factor for sharp notches.

TABLE 4 Results of the critical distance evaluation compared with Benedetti et al. [12] at 10^7 cycles

l_0 (eq. 6)	l_0 calculated using [23]	l_0 reported by Benedetti et al. [12] calculated using [23]	l_0 reported by Benedetti et al. [12] calculated $l_0 = \frac{1}{\pi}(\frac{\Delta k_{th}}{\Delta \sigma_f})^2$
$[mm]$	$[mm]$	$[mm]$	$[mm]$
0.056	0.066	0.180	0.031

By using the iterative procedure described by Susmel and Taylor it was possible to predict the lifetime of notched components with different stress concentration factors (i.e. $k_t = 2.19$ and $k_t = 1.58$).

For each experimental fatigue test, the value of the number of cycles to failure N_{fE} is substituted into eq. 5 to obtain critical distance; the linear-elastic stress distribution near the notch root (i.e. eq. 2) is used to calculate the effective stress, σ_{eff}, at the critical distance l_0 from the notch root according to the line method. In a next step, by inverting eq. 3, the predicted number of cycles to failure N_{fp} corresponding to σ_{eff} can be calculated. The procedure is iterated until the difference between N_{fp} and N_{fE} is smaller than a specific tolerance. For the present study iterative process was interrupted if the difference between the N_{fE} and N_{fp} resulted in a lesser value than 10%.

Figure 8a shows, on a double logarithmic scale, the comparison between the experimental number of cycles to failure and the predicted ones using the aforementioned procedure. From the graph it is clearly visible that the iterative process is able to generate reliable predictions for high stress concentration factors. In fact, the predictions made for $k_t = 3.09$ and $k_t = 2.19$ are within the ±3 life factors region. On the other hand, poor predictions have been obtained for $k_t = 1.58$ as the N_{fp} are outside the ±3 life factors region. This phenomena can be attributed to the poor ability of critical distance theories to account for notch size effect. In fact, the line method significantly underestimates the L-PBF Ti6Al4V fatigue life of components with a relatively low notch factor.

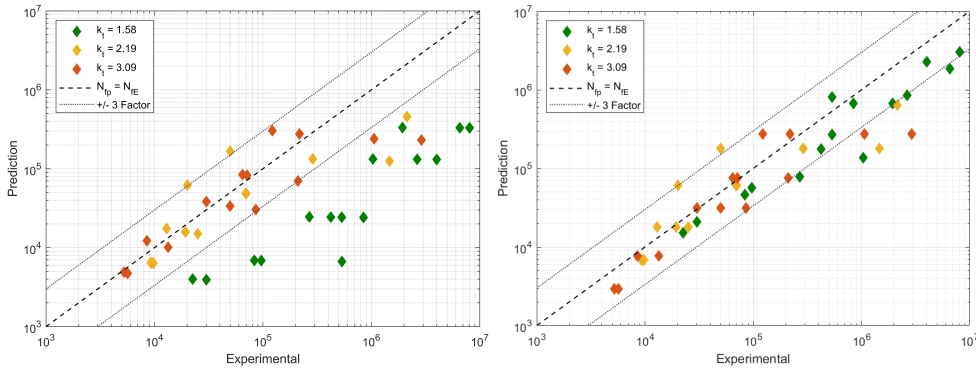

FIGURE 8 Number of cycles predicted N_{fp} by the use of the line method compared with the experimental number of cycles N_{fE}. a) N_{fp} are predicted without size effect compensation and b) N_{fp} predicted compensating for size effect

Unlike that presented in Figure 8a, in the work of Benedetti et al. the predictions made using the critical distance to assess the fatigue properties of blunt notched components were satisfactory. In their study, the defect sensitivity prevails over geometrical discontinuities sensitivity, overshadowing any type of size effect, with the fatigue failure in both sharp and blunt notches mainly driven by defect size.

For homogeneous materials, like the stress-relieved Ti6Al4V of the present study, the fatigue failure is driven by the combination of microstructural features and modified stress fields generated by the notch geometry. Therefore, as

the radius increases and the stress gradient decreases (Figure 3b), a possible notch size effect may occur and it should be included for any type of fatigue life predictions. In order to account for this phenomena, several methods have been proposed [25, 26] but none of them provided satisfactory results for the present study. Therefore, to account for the notch size effect on the critical distance, the following relationship is proposed:

$$l_n = \frac{\gamma e^{\frac{\rho}{\rho_0}}}{N_f^{\delta}} + l_0 \tag{6}$$

in which l_0 is the asymptotic critical distance calculated for $k_t = 3.09$ specimens using eq. 5 at 10^7 cycles, ρ_0 is the reference radius ($\rho_0 = 0.25mm$), ρ is radius of the notched components intended to be predicted and l_n is the critical distance that accounts for the size effect. The parameters γ and δ are determined using non-linear least square fitting.

By integrating eq. 6 in the iterative procedure it becomes possible to perform predictions for the two different batches with different notch radii. Results of Figure 8b show a significant improvement in terms of prediction capabilities, including the possibility to account for notch size effect, with the predictions N_{fp} for $k_t = 1.58$ being within the ± 3 life factors region.

| Notch sensitivity

In general the notch sensitivity factor q, defined as

$$q = \frac{k_f - 1}{k_t - 1} \tag{7}$$

is a means to express how a material reacts to a geometrical discontinuity, with $0 < q < 1$. If the notch has no effect on the material fatigue behaviour (i.e. $k_f = 1$ or $k_t \gg k_f$) then $q = 0$. On the contrary, $q = 1$ if the fatigue notch factor equals the stress concentration factor $k_t = k_f$. In this case the geometrical notch has a high impact on the material fatigue behaviour.

Focussing on the high cycle fatigue regime (i.e. $N_f = 10^7$), it can be noticed that the stress concentration factor k_t plays an important role for the notch sensitivity as an increase in k_t produces a lower notch q factor calculated using eq. 7 (Table 5). This behaviour can be explained by relating microstructural features with the stress field generated by the geometrical discontinuities.

TABLE 5 Notch sensitivity calculated at 10^7 cycles

k_t	k_f	q	$Ng_{5\%}$	S_a
1.58	1.34	0.59	32.18	0.0027
2.19	1.64	0.54	9.76	0.0121
3.09	1.94	0.45	4.88	0.0340

| Combined effect: grain size and stress distribution

It is possible to correlate the microstructural characteristics, such as the α width, the notch sensitivity factor q and the principal stress distribution at notch root with eq. 8 and 9 introduced by Peterson [27, 28].

$$q = a_p + b_p log(Ng_{5\%}), Ng_{5\%} = number\ of\ grains\ within\ 5\%\ of\ the\ maximum\ stress \tag{8}$$

$$q = c_p + d_p log(S_a), S_a = \frac{Stress\ gradient\ at\ Peak\ stress * grain\ size}{fatigue\ strength\ at\ 10^7 cycles} \tag{9}$$

where a_p, b_p, c_p and d_p are fitting coefficients determined using non-linear least square fitting.

Peterson attributed a primary importance to the region where the peak stress occurs in a notched component and that different results should be expected when this region contains different number of grains. In particular, the stressed region to within the 5% of the peak stress was accounted as region of interest.

This has also been the main motivation for the so called "highly stressed volume methods" initially developed by Kuguel et al. [29, 30] and later also successfully applied for AM metals [4, 31].

In the present study, due to the geometrical symmetry of the coupons the region of interest has been considered as the line perpendicular to the notch root, direction r of Figure 3a and the α width indicated in Table 2 is considered as the grain size. By making this assumption, the $Ng_{5\%}$ values listed in Table 3 can be considered as the number of grain boundaries that small cracks have to face before they start to propagate.

Figure 9a indicates the fatigue sensitivity factors calculated at 10^7 cycles for the three notch geometries in function of $Ng_{5\%}$. From this graph, the coefficients of eq. 8 can be determined.

It can be noticed that the notch sensitivity factor q becomes higher when the $Ng_{5\%}$ increases. The cases analysed in this study indicate that L-PBF Ti6Al4V with a fine $\alpha + \beta$ microstructure results in higher sensitivity to larger radius (i.e. $\rho = 1.5mm$, $k_t = 1.58$). A possible reason for that can be extracted by the analysis of eq. 9 and Figure 9b. In this case the notch sensitivity factors have been related to the stress gradient at the notch root, the grain size and the fatigue strength of the notched batches at 10^7 cycles. In this case, the notch sensitivity factors have been expressed in function of the quantity S_a that relate the stress gradient at peak stress with the grain size and the fatigue

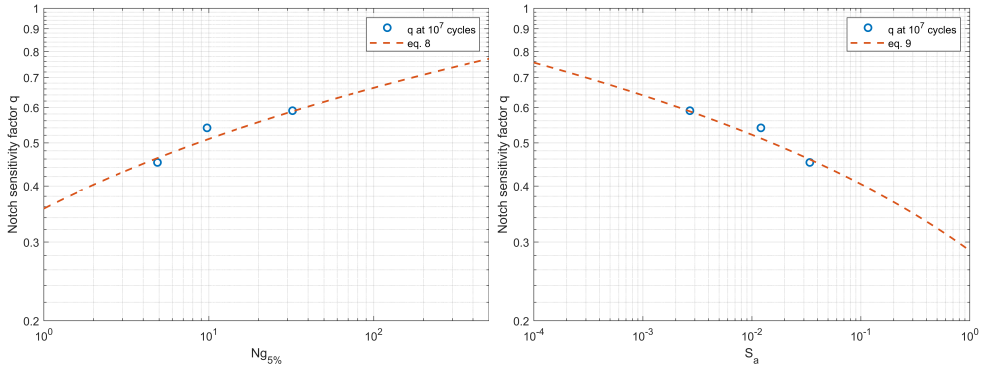

FIGURE 9 a) q in function of the number of grains within the 5% of the peak stress; b) q in function relative decrement of stress across one grain

strength at 10^7 cycles (eq. 9). S_a can be interpreted as the stress reduction occurring across each grain. For high stress concentration factors k_t, a high stress gradient is noticed at the notch root. This implies that each grain is exposed to a larger drop in stress if comparing large and small notch radius. Therefore, notched specimens with large stress drop across one grain, that can be caused either by coarse-grained material (different microstructure) or steep stress gradient (higher k_t), can be considered less notch-sensitive. In fact fatigue small cracks in these conditions encounter more difficulties propagate [27, 28].

The two empirical laws presented here could be used to study the notch sensitivity of other types of notch discontinuities and/or L-PBF Ti6Al4V with different microstructure sizes (i.e. coarse $\alpha + \beta$ generated by hot isostatic pressing). Moreover it could be possible to analyse the fatigue properties of L-PBF Ti6Al4V specimens in as-produced surface condition. In fact the wavy morphology of the as-produced surface could be treated as succession of micro-notches generated by the manufacturing process. By reconstructing the micro-notches geometry via micro computed tomography ($\mu - CT$) it could be possible to evaluate the stress-field at the micro notch root and calculate the S_a factor and compare the notch sensitivity factor q with the one evaluated with eq. 9. In order to prove this concept a dedicated $\mu - CT$ analysis of fatigue test specimens followed by fatigue test campaign would be the natural follow-up of the present study.

4 | CONCLUSIONS

In the present work the fatigue notch sensitivity of Ti6Al4V specimens produced by L-PBF and subjected to stress-relieving and machining operations has been assessed. Based on the analysis of the experimental results the following conclusions can be summarised as it follows:

- Fatigue performances of L-PBF Ti6Al4V are strongly influenced by geometrical discontinuities. The increase of the stress concentration factor k_t leads to an increase of the fatigue notch factor k_f and, consequently, to a decrease of the notch sensitivity factor q with $k_t = 3.09$ leading to $q = 0.44$.
- The critical distance l_0 has been calculated using the line method for the highest notch factor $k_t = 3.09$. The results are in line with the values obtained via threshold stress intensity factors measurements reported in literature by other authors for L-PBF Ti6Al4V with a similar microstructure.
- By using the theory of the critical distance, formulated according to the line method, it was possible to predict the fatigue life of notched specimens. The predictions were satisfactory for geometries with a high notch factor k_t, whereas poor results were obtained for relatively low k_t. The reason for that has been attributed to a notch size effect.
- In order to account for the notch size effect, a relation between the critical distance and the notch radius has been proposed. By integrating this relation in the prediction process, the final accuracy improved for the blunt notch geometry investigated.
- Given the high quality of the produced components, the failures of the samples is mainly influenced by a combination between the stress distribution generated by geometrical discontinuities and microstructural features. Therefore the material notch sensitivity can be mainly linked to these two factors. In this regard, two empirical equations are proposed to relate the modified stress distribution, the grain size and the fatigue notch sensitivity factor q. These empirical relations provided an explanation to the notch sensitivity q drop in function of the increase of the stress concentration factor k_t. In fact, specimens with a large stress drop across one grain were found to be less sensitive with respect to notched components that presented a lower drop in stress across one grain.

Acknowledgement

The authors would like to acknowledge the financial support of SIM (Strategic Initiative Materials in Flanders) and VLAIO (Flemish government agency, Flanders Innovation & Entrepreneurship) through the M3-FATAM project (*HBC*.2016.0446), part of the MacroModelMat (M3) research program, coordinated by Siemens (Siemens Digital Industries Software, Belgium).

References

references

[1] Kruth JP, Levy G, Klocke F, Childs THC. Consolidation phenomena in laser and powder-bed based layered manufacturing;56(2):730–759.

[2] Li P, Warner DH, Fatemi A, Phan N. Critical assessment of the fatigue performance of additively manufactured Ti–6Al–4V and perspective for future research;85:130–143. http://www.sciencedirect.com/science/article/pii/S0142112315004399.

[3] Leuders S, Thöne M, Riemer A, Niendorf T, Tröster T, Richard HA, et al. On the mechanical behaviour of titanium alloy TiAl6V4 manufactured by selective laser melting: Fatigue resistance and crack growth performance;48:300–307. http://www.sciencedirect.com/science/article/pii/S014211231200343X.

[4] Van Hooreweder B, Moens D, Boonen R, Kruth JP, Sas P. Analysis of fracture toughness and crack propagation of Ti6Al4V produced by selective laser melting. Advanced Engineering Materials 2012;14(1-2):92–97.

[5] Elangeswaran C, Cutolo A, Muralidharan GK, de Formanoir C, Berto F, Vanmeensel K, et al. Effect of post-treatments on the fatigue behaviour of 316L stainless steel manufactured by laser powder bed fusion;123:31–39. http://www.sciencedirect.com/science/article/pii/S0142112319300143.

[6] Elangeswaran C, Cutolo A, Muralidharan GK, Vanmeensel K, Van Hooreweder B. Microstructural analysis and fatigue crack initiation modelling of additively manufactured 316L after different heat treatments;194:108962. http://www.sciencedirect.com/science/article/pii/S0264127520304962.

[7] Molaei R, Fatemi A, Sanaei N, Pegues J, Shamsaei N, Shao S, et al. Fatigue of additive manufactured Ti-6Al-4V, Part II: The relationship between microstructure, material cyclic properties, and component performance;132:105363. http://www.sciencedirect.com/science/article/pii/S0142112319304670.

[8] Kahlin M, Ansell H, Moverare JJ. Fatigue behaviour of notched additive manufactured Ti6Al4V with as-built surfaces;101:51–60. http://www.sciencedirect.com/science/article/pii/S0142112317301809.

[9] Razavi SMJ, Ferro P, Berto F, Razavi SMJ, Ferro P, Berto F. Fatigue Assessment of Ti–6Al–4V Circular Notched Specimens Produced by Selective Laser Melting;7(8):291. https://www.mdpi.com/2075-4701/7/8/291.

[10] Razavi SMJ, Berto F. Directed Energy Deposition versus Wrought Ti-6Al-4V: A Comparison of Microstructure, Fatigue Behavior, and Notch Sensitivity;21(8):1900220. https://onlinelibrary.wiley.com/doi/abs/10.1002/adem.201900220, _eprint: https://onlinelibrary.wiley.com/doi/pdf/10.1002/adem.201900220.

[11] Cutolo A, Elangeswaran C, de Formanoir C, Muralidharan GK, Van Hooreweder B. Effect of Heat Treatments on Fatigue Properties of Ti–6Al–4V and 316L Produced by Laser Powder Bed Fusion in As-Built Surface Condition. In: TMS 2019 148th Annual Meeting & Exhibition Supplemental Proceedings The Minerals, Metals & Materials Series, Springer International Publishing;. p. 395–405.

[12] Benedetti M, Santus C. Notch fatigue and crack growth resistance of Ti-6Al-4V ELI additively manufactured via selective laser melting: A critical distance approach to defect sensitivity;121:281–292. http://www.sciencedirect.com/science/article/pii/S0142112318307084.

[13] Molaei R, Fatemi A, Phan N. Notched fatigue of additive manufactured metals under axial and multiaxial loadings, Part I: Effects of surface roughness and HIP and comparisons with their wrought alloys;143:106003. http://www.sciencedirect.com/science/article/pii/S0142112320305351.

[14] Beckers A, Muralidharan GK, Lietaert K, Ray N, Van Cauwenbergh P, Vanacken K, et al. On the advances to obtain excellent and repeatable mechanical properties and build quality of LaserForm® Ti gr23 (A) across whole build platform. In: MATEC Web of Conferences, vol. 321 EDP Sciences; 2020. p. 03015.

[15] Tech specs | 3D Systems;. https://www.3dsystems.com/materials/laserform-ti-gr-23/tech-specs.

[16] Elangeswaran C, Gurung K, Koch R, Cutolo A, Hooreweder BV. Post-treatment selection for tailored fatigue performance of 18Ni300 maraging steel manufactured by laser powder bed fusion;43(10):2359–2375. https://onlinelibrary.wiley.com/doi/abs/10.1111/ffe.13304, _eprint: https://onlinelibrary.wiley.com/doi/pdf/10.1111/ffe.13304.

[17] Neuber H. Theory of notch stresses: principles for exact stress calculation of strength with reference to structural forms and materials. AEC TR 4547 1958;.

[18] Nicholas T. Step loading for very high cycle fatigue;25(8):861–869. https://onlinelibrary.wiley.com/doi/abs/10.1046/j.1460-2695.2002.00555.x, _eprint: https://onlinelibrary.wiley.com/doi/pdf/10.1046/j.1460-2695.2002.00555.x.

[19] Bellows RS, Muju S, Nicholas T. Validation of the step test method for generating Haigh diagrams for Ti–6Al–4V;21(7):687–697. http://www.sciencedirect.com/science/article/pii/S0142112399000328.

[20] Thijs L, Verhaeghe F, Craeghs T, Humbeeck JV, Kruth JP. A study of the microstructural evolution during selective laser melting of Ti–6Al–4V;58(9):3303–3312. http://www.sciencedirect.com/science/article/pii/S135964541000090X.

[21] Vrancken B, Thijs L, Kruth JP, Van Humbeeck J. Heat treatment of Ti6Al4V produced by Selective Laser Melting: Microstructure and mechanical properties;541:177–185. http://www.sciencedirect.com/science/article/pii/S0925838812011826.

[22] Susmel L, Taylor D. A novel formulation of the theory of critical distances to estimate lifetime of notched components in the medium-cycle fatigue regime;30(7):567–581. https://onlinelibrary.wiley.com/doi/abs/10.1111/j.1460-2695.2007.01122.x, _eprint: https://onlinelibrary.wiley.com/doi/pdf/10.1111/j.1460-2695.2007.01122.x.

[23] Santus C, Taylor D, Benedetti M. Determination of the fatigue critical distance according to the Line and the Point Methods with rounded V-notched specimen;106:208–218. http://www.sciencedirect.com/science/article/pii/S0142112317303948.

[24] Santus C, Taylor D, Benedetti M. Experimental determination and sensitivity analysis of the fatigue critical distance obtained with rounded V-notched specimens;113:113–125. http://www.sciencedirect.com/science/article/pii/S0142112318301294.

[25] Zhu SP, He JC, Liao D, Wang Q, Liu Y. The effect of notch size on critical distance and fatigue life predictions;196:109095. http://www.sciencedirect.com/science/article/pii/S0264127520306304.

[26] Yang X, Wang J, Liu J. High temperature LCF life prediction of notched DS Ni-based superalloy using critical distance concept;33(11):1470–1476. https://www.sciencedirect.com/science/article/pii/S0142112311001423.

[27] Peterson R. Methods of correlating data from fatigue tests of stress concentration specimens. Stephen Timoshenko Anniversary Volume 1938;p. 179.

[28] Peterson R. Relation between life testing and conventional tests of materials. Bulletin ASTM 1945;(133).

[29] Kuguel R. The highly stressed volume of material as a fundamental parameter in the fatigue strength of metal members. University of Illinois. A M Report 1960;169.

[30] Kuguel R. A relation between theoretical stress concentration factor and fatigue notch factor deduced from the concept of highly stressed volume. In: proc. ASTM, vol. 61; 1961. p. 732–748.

[31] Van Hooreweder B, Boonen R, Moens D, Kruth JP, Sas P. On the determination of fatigue properties of Ti6Al4V produced by selective laser melting. In: 53rd AIAA/ASME/ASCE/AHS/ASC Structures, Structural Dynamics and Materials Conference 20th AIAA/ASME/AHS Adaptive Structures Conference 14th AIAA; 2012. p. 1733.